Distinct element modelling and mining induced subsidence : Influence of the major faults
Modélisation des affaissements miniers : Influence des failles
Die verschiedenen Elemente Methode und Bergbaubodensenkung : Einfluss der Verwerfungen

F. Homand-Etienne, I. Mamane, M. Souley
Laboratoire de Géomécanique, ENSG, Vandoeuvre-lès-Nancy, France

P. Gaviglio
Laboratoire de Géologie Structurale et Appliquée, Université de Besançon, France

M. Al Heib
Laboratoire de Mécanique des Terrains - INERIS, Ecole des Mines, Nancy, France

ABSTRACT : This study examines the subsidence due to underground mining works in a coal mine in France. Coal is mined at a depth reaching 1000 m, according to longwall face method with caving. The seam ranges between 2 and 3.4 m in thickness. The dip strata does not exceed 10°. As predicted by the empirical curves, the numerical and measured maximum subsidence does not exceed 70% of seam thickness. Numerical modelling and empirical methods overestimate the subsidence for extracted longwall width greater than 700 m.

RÉSUMÉ : Cette étude des affaissements induits par l'exploitation de charbon a été faite pour une mine située à une profondeur de 1000 m en France. La puissance de la couche exploitée par longue taille varie de 2 à 3,4 m et le pendage des strates ne dépasse pas 10°. Comme le prédisent les courbes empiriques, l'affaissement maximal mesuré ou calculé numériquement n'excède pas les 70% de l'ouverture. Pour des largeurs exploitées supérieures à 700 m, les valeurs mesurées sont nettement inférieures à celles calculées.

ZUSAMMENFASSUNG : Diese Untersuchung der durch Kohlegewinnung induzierten Bodensenkung ist in dem Rahm eine 1000 m tief französische Zeche durchgeführt. Die Mächtigkeit des durch Strebenmethod abgebauten Flöz variiert zwischen 2 und 3,4 m. Die Längsneigung der Schichten ist nicht grösser als 10°. Wie von empirischen Kurven vorausgesehen überschreitet die abgemessene oder berechnete Höchstsenkung 70% der Mächtigkeit nicht. Für über 700 m abgebauten Breiten sind die abgemessenen Werte entschieden geringer als die berechneten Werte.

1 INTRODUCTION

Knowledge of subsidence engineering is of considerable importance to the planning and development of surface. Subsidence is generally associated with the extraction of minerals and natural resources such as oil, gas and water. It is vital for population to be aware of the risk of possible surface collapses above the underground openings. In such situations, knowledge should be established. Prediction methods exist for determining the likely magnitude and extent of subsidence development at the surface. These methods include empirical, numerical and analytical approaches. Empirical methods were essentially based on experience and field measurements. There are intended to similar other sites. Also, surface subsidence has been predicted using a number of numerical models based predominately on simplified elastic and isotropic assumptions. Many of these methods appear to make assumptions that are invalid and, consequently, give results which oversimplify subsidence prediction.

The main objective of this study is to compare analytical, empirical and numerical methods for a specific site *(Provence Colliery)* in which the subsidence data were available, with intent to valid the methods of modelling and to evaluate their estimated character in relation to new sites. Empirical or analytical methods can not take into account some local phenomena well known as *flight of stairs* near faults. The numerical modelling, especially the one based on the Distinct Element concepts, allows for the presence of discontinuities, therefore permits to display prominently the relative movement of discontinuities and to analyse more accurately this movement. The special feature of the numerical modelling presented here is that we have taken into account the tectonic history affecting the site during the loading sequences. Numerical analyses described in this paper were conducted using the two-dimensional UDEC code.

2 GEOLOGICAL CHARACTERISTICS OF BASIN

The coalfield under investigation belongs to the *Gardanne* basin, which forms the eastern part of the Arc basin, and is an E-W oriented geological unit located 10 km north of Marseille.

The geological structure is simple : the asymmetric syncline is strongly affected by a dome-shaped anticline (Fig. 1). In the presently mined area, the structure is overridden by a major thrust sheet overthrusting Northward (Etoile unit), due to the North-South shortening and the major tectonic event of the geological history of the region. The same episode is responsible for strike-slip faulting all over the area (Gaviglio *et al.* 1990).

The lignite seams belong to the *Fuvelian* (upper part of the *Campanian*), sequence which is made up of limestone. This occurrence of coal amid calcareous beds is major geological particularity of the coalfield, and is responsible for the great difference in mechanical stiffness between the coal seam and the calcareous beds forming the floor and roof. The *Fuvelian* limestones are 250 m thick in the mining zone.

SW   NE
Etoile overthrust   Diote fault

2km

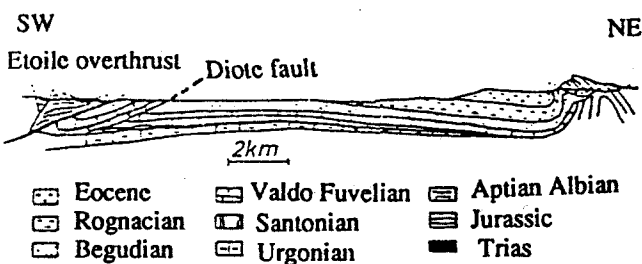| ▦ Eocene | ▦ Valdo Fuvelian | ▦ Aptian Albian |
| ▦ Rognacian | ▦ Santonian | ▦ Jurassic |
| ▦ Begudian | ▦ Urgonian | ▬ Trias |

Fig.1-Geological cross section (Gaviglio *et al.* 1990).

The investigated zone lies in the autochthonous part of basin, just in front of the tectonic thrust wedge and bounded by the *Diote* fault and the *Safre* fault. Numerous detailed geological studies have been conducted in this region, but little attention has been paid to the fracturing pattern. However, due to underground workings in the lignite field, detailed structural data are now available. To illustrate this, a highest density of faulting lies southward in the vicinity of the *Safre* fault : this zone has directly undergone the compressive load exerted by the thrust sheet. Also, the geological history is responsible for the present state of stress, the variation of the physical and mechanical properties of the calcareous bed, and the geometrical arrangement of the major faults planes. The principal fault planes may have an influence on the behaviour of the strata, through their geometrical characteristics, especially if their effects combine (Gaviglio *et al.* 1990). This is also, confirmed in a recent study reported by Mamane (1995).

Above the *Grande Mine*, the overburden is made up of *Fuvelian, Begudian, Rognacian* and *Eocene*, below the *Fuvelian* lie *Cretaceous* and *Jurassic*. The coal seam is 1000 m deep and dips East-West at an angle of 8°. The thickness of worked seam varies between 2 and 3 m. Above and below the coal seam, the rock is stratified and consists of very tough beds of limestone.

3 EMPIRICAL PREDICTION METHODS

In these methods, the maximum subsidence (W_m) is calculated based on the extracted seam height (O), the goaf treatment coefficient (q), the nature of cover rocks and depth (H).

Concerning the influence of longwall width on the maximum subsidence, it seems that the model which is successfully utilised is based on the use of an empirical curve relating the depth (H) to the longwall width (L), as follows :

$$\frac{W_m}{O} = \frac{L}{H} \tag{3.1}$$

Fig. 2 shows the maximum subsidence expressed in terms of extracted seam height and results have been plotted against the ratios of the extraction width over depth below surface (L/H). Fig. 2 represents also the *Provence Colliery* empirical curves. Note that these curves are qualitatively similar to those obtained in other countries as reported by Whittaker & Reddish (1993). However, observations of mining subsidence reported in several countries have shown that the maximum subsidence above the longwall extraction can be appreciably influenced by the nature of the cover rocks. Another feature illustrated in this figure is : the form *"S"* of the empirical curve which corresponds to three distinct parts (Arcamone 1980) :

• The starting of *"S"* corresponds to the first effects of subsidence. The maximum subsidence W_m does not exceed 10% of the extracted seam height (O), for widths extraction involving L/H ratios which lie within of 0-0.4. Subsidence is essentially related to the settling of cover rocks. This part of curve represents a highly effective control parameter of the magnitude of surface subsidence.

• The linear part of curve corresponds to the actual setting of subsidence due to the collapses of cover rocks. In *Provence Colliery*, W_m varies between 10 and 60% of extracted seam height H, for L/H within 0.4-1.2.

• The third part of *"S"* corresponds to the final equilibrium. An important feature of this part (in *Provence* case) is that, for L/H greater than 1.2 ; the value of W_m/O tends towards a constant of 0.6-0.7. In others words, the maximum subsidence does not exceed 70% of extracted seam height in *Provence Colliery* case.

In order to predict the shape of subsidence profiles trough for mining dimensions, many authors have proposed some form of equation or graph. Equations may be simple or complex, but generally based on results obtained from case studies. These profiles are all of the form :

$$W(x) = W_m f(\gamma, x, H, C) \tag{3.2}$$

where W_m is the subsidence at the centre of trough, γ is the critical angle, H is the mining depth, x is the horizontal distance from the centre of extracted longwall and C is the profile function constant which is adjusted until a best fit image with the measured profile is obtained.

It is clearly established that geological and hydro-geological factors play a major role on the nature and magnitude of subsidence induced by mining. Also, the empirical methods used for subsidence prediction are unable to take into account the effect of faults on the ground surface movements.
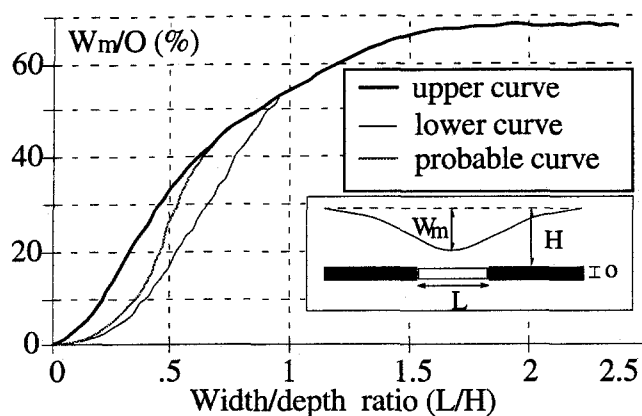

Fig. 2 - Empirical relationship between the magnitude of subsidence expressed in terms of extracted seam height and longwall width/depth ratio for coal mining operations at the *Provence Colliery*(Arcamone 1980).

4 NUMERICAL MODELLING

4.1 Models and loading sequence

As reported in § 2, the area is constituted of *Jurassic, Fuvelian, Begudian* and *Rognacian*. In the mined area, the major tectonic events are at the root of variety of fractures, and an accurate study performed by Gaviglio (1985) was permitted to define the main fracture trends. In particular, three major reverse faults : *Diote, Etoile* and *Safre* form the structure at the southern part.

The two-dimensional geometrical model used to simulate a cross section that strikes North-South, is based on the geological cross section of the basin and illustrated in Fig. 3, with respect to the average coal seam dip. The area of interest for the modelling of the *"Grande Mine"* site is about 4 km long and the model depth chosen is 1.2 km. The deposit is 950 m deep, the height of coal seam is 3 m and the dip strata is 8°. Mining is simulated by instantaneous excavation of 100 m of coal at every step and the excavation of the entire longwall cross section corresponds to 1000 m.

In situ stress measurements were carried out in the mine workings. These investigations have demonstrated that the major principal stress is always horizontal, and is much higher (2 to 3 times) than the minor principal stress (σ_3), whereas the intermediate stress is almost vertical $(\sigma_2=\sigma_v)$. Also, the vertical stress is, in any case, smaller than expected from the weight of overburden (0.53 to 0.87 times). In other respects, a recent study reported by Mamane (1995) showed that the in situ stress state results from the combination of the gravity and the participation of tectonic stresses. For these reasons, we performed two models : Model A without tectonic stress consideration and which represents the present-day conditions, and Model B involving both gravity loading and a North-South tectonic compression to the value of 5 MPa $(\sigma_s=5MPa)$.

The modelling sequences are performed as follows : *firstly*, both models (A and B) without excavation were consolidated under *in situ* stresses (Fig. 4b), *secondly*, for model B a compressive tectonic stress is applied as illustrated in Fig. 4b, and *thirdly*, the excavation was carried out (roller boundaries were applied to the sides and the base of the both models) and models were cycled to an equilibrium state for stress redistribution. Notice that the boundary conditions used during tectonic loading relate the geological history of the region as reported by Gaviglio (1985).

The rock mass is modelled using the fully deformable blocks assumption. Rock blocks are assumed to be isotropic and linearly elastic materials. In fact, different materials in *Provence Colliery* behave elastically (Gaviglio 1987), even if materials overburden the *Begudian-Rognacian* at the surface are constituted to clay materials which can behave in an elastic-plastic manner.

4.2 Choice of materials and joints characteristics

Concerning the mechanical properties of rock materials, *Provence* site is constituted of three major sets of materials, though in the lithologic point of view, the basin is formed of five groups (*Jurassic, Fuvelian, Begudian, Rognacian* and *Eocene*). Material number of these sets are illustrated in Table 1. Mechanical characteristics of these materials also reported in Table 1, are derived from laboratory tests.

Table 1 - Elastic properties of rock materials.

ROCK MATERIALS	ν	E (MPa)
BEGUDIAN	.25	3000
FUVELIAN	.25	24000
JURASSIC	.25	37000
COAL	.30	2000

Fig. 3 - Geometrical model based on the geological cross section of the basin.

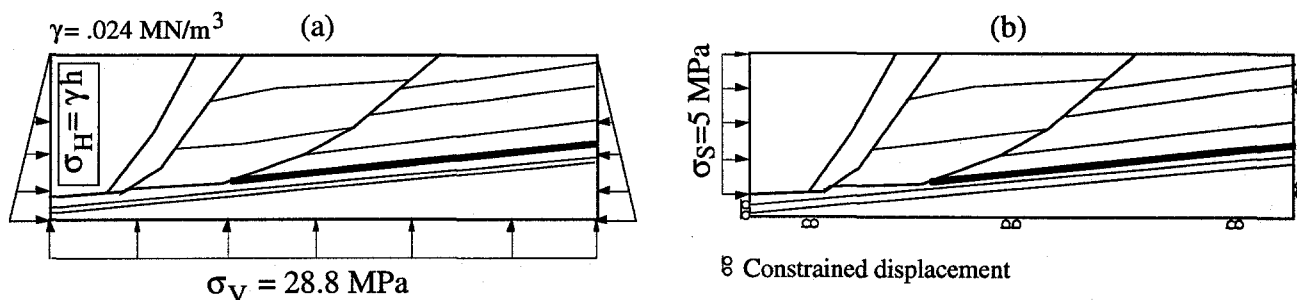| 1 : Begudian-Rognacian | 3 : Jurassic |
| 2 : Fuvelian | ▬▬ *Grande Mine* seam |

Fig. 4 - Loading and boundary conditions : (a)-models loading using gravity, initial *in situ* stresses and boundary stresses (b)-tectonic loading and boundary conditions during excavation.

Unlike the rock mass properties, it was not possible to deduct in advance the mechanical properties of joints (faults and joints between materials). Therefore, the choice of these parameters presented here is based on some approaches encountered in the literature. The normal and shear stiffness k_n and k_s during the consolidation were calculated based on a recent study reported by Kulatilake *et al.* (1992). In this approach, k_n and k_s depend essentially on the elastic properties of rock materials. Computed values are reported in Table 2. Concerning k_n and k_s needed for joints during tectonic compression and excavation, it is clearly established that the mechanical behaviour of joint is generally non-linear and depend on large parameters such as : stress level, dilatancy, weathering state of joints, joint wall geometry, strength and deformability of asperities. Based on the relationships suggested by Bandis *et al.* (1983) and assuming that all joints have no dilatancy and their compressive strength *(JCS)* is equal to the uniaxial compressive strength of rock materials, the initial normal stiffness, the maximum normal closure and the shear stiffness for each discontinuity were calculated. Therefore it is possible to derive the normal stiffness *(kₙ)* according to the normal stress level and the hyperbolic model of Bandis *et al.* Finally, joints parameters used during tectonic loading and excavation are also, summarised in Table 2.
We assume that normal and shear behaviour of joints are linear and the shear stress is limited by Mohr-Coulomb's criterion.

Table 2 - Mechanical properties of joints.

| Joint materials | DURING | | | | |
| | Consolidation | | Excavation | | |
	k_n^*	k_s^*	k_n^{**}	k_s^{**}	$\phi(°)$
1	188	75	3000	7.5	20
2	2625	1050	25000	100	22
3	200	80	2500	8	20

* GPa/m; ** MPa/m; ϕ is joint friction angle.
1- *Begudian/Fuvelian, Begudian/Begudian, Begudian/Jurassic*
2- *Fuvelian/Fuvelian, Fuvelian/Jurassic*
3- *Coal/Fuvelian, Coal/Coal, Coal/Jurassic.*

4.3 Results

We then analysed the mining induced movements of ground surface with respect to extracted longwall width according to model A which represents the present-day conditions. A qualitative and quantitative comparison between models A and B was also performed.
Fig. 5 shows the magnitude of subsidence expressed in terms of height *(Wₘ/O)* and the longwall width/depth ratio *(L/H)*, compared to pre-established empirical curves. This indicates that values of W_m/O ratio have to fall between the lower and upper empirical curves, except for large values of extracted longwall width *(L≥800 m)*. In spite of the fact that the model overestimates (much less than 7% of extracted seam height : *O*) values of W_m for *L≥800*, it is interesting to note that the maximum magnitude of subsidence does not exceed 70% of extracted seam

height ; this is agreed with field observations. Also, Fig. 5 illustrates that the calculated values of W_m are virtually identical with those obtained according to probable curve for $L \leq 400$, whereas difference between simulated and empirical curves does not exceed 8% of coal seam height, for extracted width ranged between 500-700 m. Consequently, based on these observations, we note a good agreement between simulated and empirical curves.

Fig. 6 shows curves of ground surface subsidence $W(x)$, with respect to L. These subsidence profiles lead to the following comments : *(i)* - $W(x)$ increase with the extracted width and the point of maximum subsidence (i.e. M in Fig. 6) moves from north to south when the face advances. However, as illustrated in Fig. 6, this point is not located in the middle of extracted zone (which represents the theoretical point of maximum subsidence) due to the face advance, behaviour of discontinuities and inclination of coal seam. *(ii)* - No significant effect of *Diote* fault is observed at the surface when $L \leq 600$ compared to *Etoile* and *Safre* faults influence clearly marked in Fig. 6.
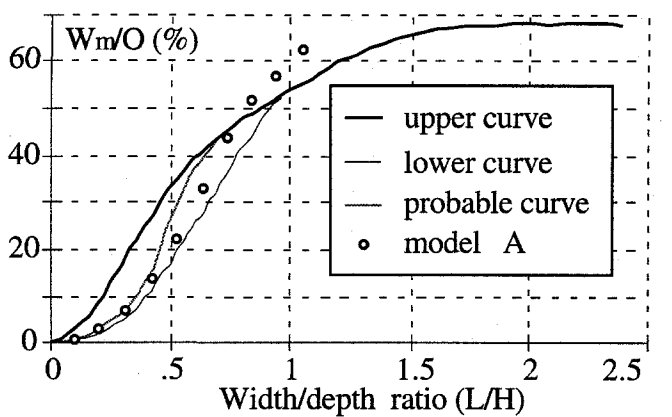

Fig. 5 - Calculated curve for subsidence with respect to the advancing face compared to empirical curves.

Also, interpretation of results when $L \geq 700$ shows that while *Diote* fault increases the magnitudes of subsidence, *Safre* and *Etoile* faults tend on the contrary, to reduce the subsidence at the northern side of *Safre* fault. In other terms, *Diote* fault effects take place after 700 m of extracted longwall width and tend to reduce the *Etoile* and *Safre* faults effects. This is clearly marked for $L=1000$ in Fig. 6. In order to explain this faults inter-influence with respect to the advancing face, we analysed the behaviour of faults according to extracted width.

Fig. 7 shows the direction of block movements and shear displacement through discontinuities at the roof corresponding to $L=200$. Examination of these displacements with respect to L has demonstrated when the extracted width increases, points A, B, C and D reported in Fig. 7 tend to move from north to south, whereas the point E located along *Diote* fault moves towards the excavation. In particular, when $L \geq 700$, all joints located at the roof and dipped about 8° have a *dextral* movement. Consequently, *dextral* movement occurs along *Fuvelian-Begudian* interface (2/1), whereas *Fuvelian-Fuvelian* joint (2/2) tends to open due to an increase of inflexion of *Fuvelian* bed at the immediate roof with increase of extracted width. Also, the part of *Diote* fault overburden the immediate roof *Fuvelian* has a *dextral* movement, while *Etoile* and *Safre* faults have a *normal* displacement, but these both faults are *reverse* in depth. Effectively, behaviour of *Safre* and *Etoile* faults has conditioned the evolution (virtually linear) of subsidence in the *Begudian* block delimited by these two faults as illustrated in Fig. 6.
Note that $L=700$ represents the minimum extracted longwall width provoking an entire collapse of roof,
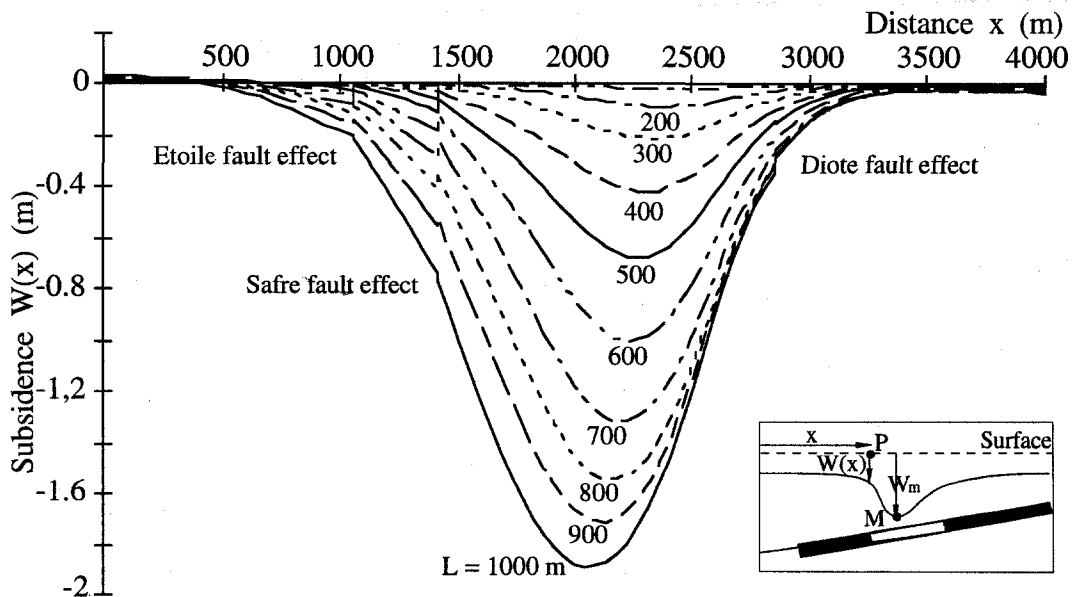

Fig. 6 - Subsidence results; illustrating the influence of the extracted longwall width.

whereas extraction of 600 m of coal seam induces a maximum roof-floor convergence about 1.9 m.

Evolution of surface horizontal displacement $U(x)$ curves with respect to L is illustrated in Fig. 8. As observed earlier in subsidence analysis, magnitudes of horizontal displacements increase with extracted width and the point of maximum subsidence (intersection of displacement curve and horizontal axis) move from north to south. Also, Fig. 8 illustrates the great part of faults in ground movements. Heaves of *Diote, Safre* and *Etoile* faults express fault opening at the surface. It is interesting to note that contrary to *Safre* and *Etoile* effects on the subsidence profiles (reducing) observed in Fig. 6 for $L{\geq}700$, Fig. 8 indicates an accumulation of *Safre* and *Etoile* effects on the horizontal displacements. It should be noted that constant horizontal displacement of *Jurassic* block delimited by *Safre* and *Etoile* faults clearly indicates that this block behave as a rigid block, therefore practically governed by the faults deformability as explained earlier.

Differential movements of the ground surface produces ground strains, and damage of surface structures is generally correlated to the magnitude of these strains. Examination of the horizontal and vertical strain curves (i.e. dU/dx and dW/dy) not presented here, showed that simulated curve forms are similar to those encountered in the literature. In particular, horizontal strain curves show two distinct parts : *(i)* compressive strain part, around the point of maximum subsidence, *(ii)* tensile ground strains on both sides of the previous compressive strain region. Maximum compressive strain (E_{max}) obtained at the excavation of the entire longwall $(L=1000)$ is about 1.69 mm/m which approaches the theoretical value given by the empirical relation : $k\ W_m/H$ (where k is constant ranged between 0.8 and 1.5). About maximum slope of ground surface (vertical strain) and curvature obtained by differentiating the subsidence profile, we got respectively : $T_{max}=4$ mm/m and $K_{max}=2.5\ 10^{-6}\ m^{-1}$.

Then according to the classification of Baochen (1993) applied to surface structures specifically to determine the extent of damage caused to the surface structures as a result of ground deformation, previous values of E_{max}, T_{max} and K_{max} lead to the following interpretation : structures at the surface are not very sensitive to surface movements and deformation in the case of *Provence Colliery*.
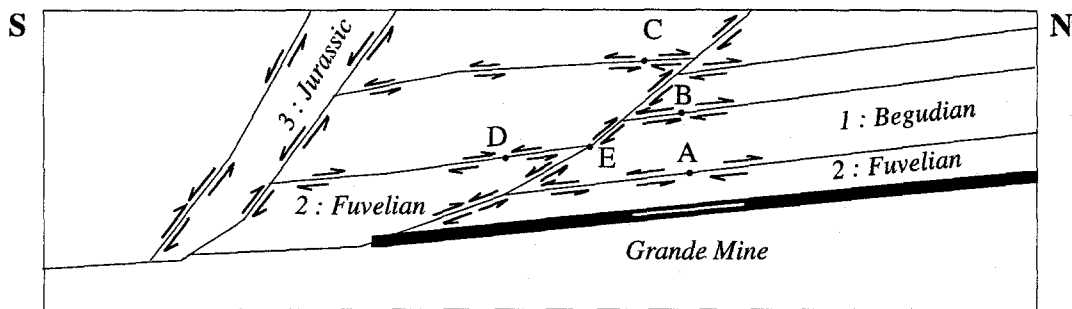

Fig. 7 - Mechanism of slip through discontinuities overhanging the *Grande Mine* coal seam $(L=200\ m)$.
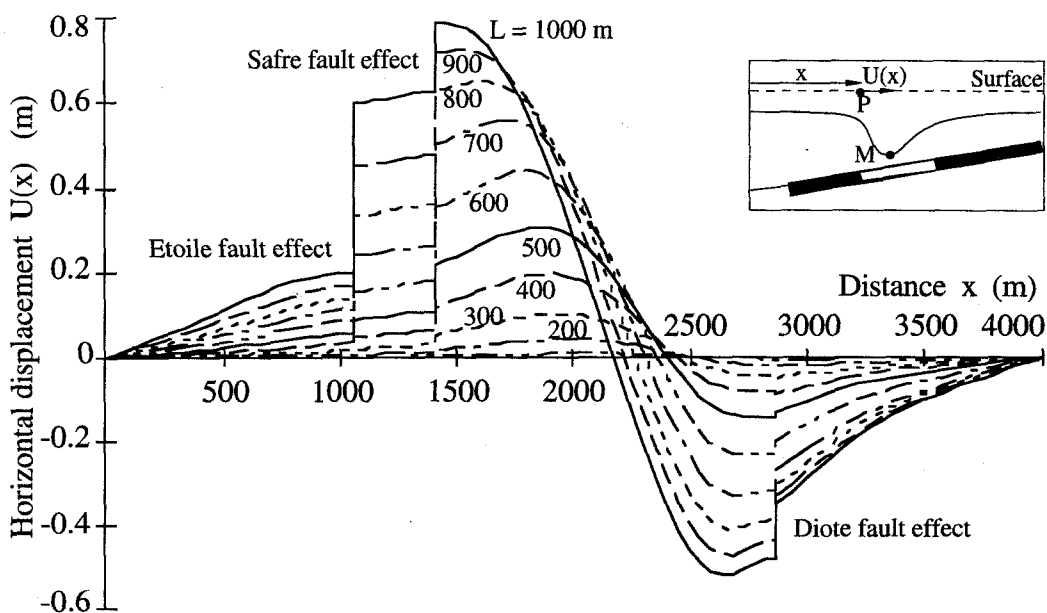

Fig. 8 - Horizontal displacement results; illustrating the influence of the extracted longwall width.

Consideration of the existing N-S tectonic compression (model B) at the end of model consolidation favours the development of shear movement through discontinuities overhanging the longwall. Value of shear displacement along *Diote* fault decreases from 0.1 m towards the seam level to 1 mm near the surface. Contrary to model A, analysis of deformability according to model B showed that fractures have *dextral* movement for extracted longwall width less than 500 m. In other words, for $L<500$, ground surface movements are appreciably influenced by the tectonic compression.

Table 3 summarises the values of W_m according to model with respect to extracted width, and indicates that N-S compression reduces the magnitudes of subsidence. Value of this reduction is about 60% for $L\leq200m$ and tends towards a constant of 5-10% when $L\geq600$. In the later cases, shear displacements along discontinuities are qualitatively similar to those observed according to model A (i.e. Fig. 7). However for extracted width $L\leq200$, the behaviour of model B is entirely governed by the applied σ_s. This has been again confirmed by the examination of displacement and subsidence profiles corresponding to $L=100-200$ m.

Table 3 - Comparison of maximum subsidence

W_m (cm)	Extracted longwall width L (m)				
	L=100	L=200	L=300	L=400	L=500
Model A	1.88	8.7	21.2	42	67.6
Model B	0.7	3.3	16	36.8	62
	L=600	L=700	L=800	L=900	L=1000
Model A	100	131.5	154.5	171	188.3
Model B	93.2	123.6	145.5	161.5	179

Similarly to W_m evolution according to model A, σ_s tends to reduce the subsidence magnitudes $W(x)$ for a given extracted width. Recall that σ_s induces *dextral* movement through faults, whereas mining workings generate a *sinistral* movement of faults. It is interesting to note that a combination of the two previous phenomena can generate another block cinematic at the surface in certain cases.

In other respects, the existing of σ_s develops a large horizontal displacement magnitudes. Contrary to model A, these horizontal displacements can approach the values of W_m. To illustrate this, value of horizontal displacement of the right side of *Safre* fault according to models B and A are respectively, 1.24 and 0.76 m. However, horizontal displacement curves are qualitatively similar to those observed in Fig. 8 particularly for $L>500$ m except in the region involving *Fuvelian* at the left hand side of model (i.e. where σ_s is applied).

Finally the existing N-S tectonic compression reduces the magnitudes of W_m and $W(x)$, and increases significantly the horizontal displacements $U(x)$ with respect to extracted longwall width.

5 DISCUSSION AND VALIDATION

5.1 Comparison with in situ measurements

The main comparisons between empirical and numerical predicted and measured maximum subsidence with respect to extracted width are illustrated in Fig. 9. Direct comparison between empirical curves and measured W_m leads to the following observations : five of eight measurements were located between the lower and upper empirical curves, whereas three measures have been overestimated by both predictions (empirical and numeric).

It may be seen that numerical maximum subsidence predicted and the measured data are in fully close agreement for three particular extracted longwall widths. The corresponding longwall width/depth ratios are 0.41, 0.43 and 0.65. Also, the measured maximum subsidence corresponding to extracted longwall width/depth ratio higher than 0.71 remains lower than one which was calculated with models A and B. However, recall that the previous ratio (0.7) corresponds to the minimum extracted width occurring an entire collapse of longwall roof, therefore inducing an increase of *Diote* fault effects as earlier observed in Figs 6 and 8.

Note that the induced subsidence and horizontal displacement at the location of *Diote* fault (i.e. relative subsidence and horizontal displacement between the left and right sides of fault) for $L=1000$ are respectively about 0.06 and 0.13 m, and increase at the point of maximum subsidence location (combination of *Diote* fault and excavation effects).

Reasons for these discrepancies between models and measurements for extracted width higher than 700 m are not clear, but possibly their are related to either variations of faults behaviour due to immediate roof collapse, and continuum movement of materials towards the longwall before the roof collapse process which depends on the extracted width. To illustrate this, an elasto-plastic analysis performed by Mamane (1995) showed that maximum subsidence is reduced due to the roof collapse which occurs before 700 m of extracted longwall, therefore continuum movement of roof in present cases will be reduced due to the actual *"artificial"* pillar.

Also, making *Diote* and *Safre* faults stiffer reduces the maximum subsidence for $L\leq800$ and increases the maximum subsidence for $L\geq900$, because in this case, roof collapse occurs with respect to 900 m of extracted width. In other words, maximum subsidence will be correlated to the critical extracted width which provokes the roof collapse.

5.2 Comparison with the model of Baochen (1993)

Analytical model of Baochen for subsidence prediction is used to valid the numerical modelling. Validation was made for 1000 m of extracted longwall width and we present the essential results.
Parameters of subsidence profiles (maximum horizontal displacement, maximum subsidence and critical angle) needed for the theoretical model, have been derived from the empirical relationships suggested by Baochen (1995).
Evolution of subsidence profile according to Baochen's theory has globally the same trend than that observed using models A or B (i.e. Fig. 6). Also, the part of analytical and numerical profiles corresponding to the right side of the longwall match qualitatively and quantitatively. Note that empirical relationship of W_m given by Baochen underestimates the maximum subsidence compared to simulations. Consequently, Baochen's model tends to underestimate the magnitudes of subsidence, particularly over the longwall. However, both points (analytical and numerical) of maximum subsidence fall in the same range.

If we had used the value of W_m obtained from our simulations in Baochen's model, results of this validation will be certainly ameliorated.
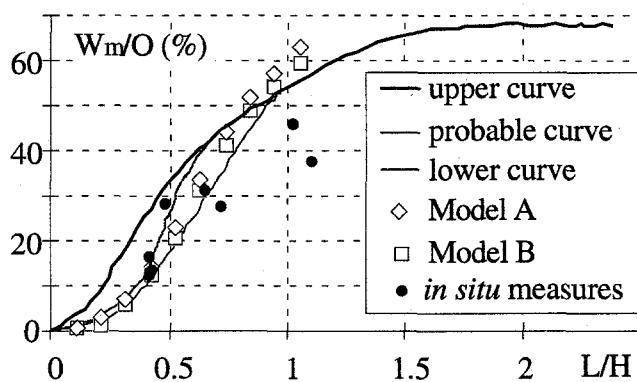

Fig. 9 - Maximum subsidence : comparison with measured data.

6 CONCLUSION

Ground surface movements due to mining workings were examined for a specific *French Coal Mine*. Results involve numerical, empirical and analytical approaches, and *in situ* measurements. Based on the analysis reported here, the main conclusions can be summarised as follows :
• We note a good agreement between simulated and empirical curves of maximum subsidence with respect to extracted width. As predicted by the empirical curves, the numerical and measured maximum subsidence does not reach 70% of seam height.
• Comparison with the *in situ* measurements has shown that five of eight measures are located between the lower and upper curves and consequently agree with the values predicted by calculations. However, significant discrepancies between numerical and empirical predictions on the one hand, and observed measurements on the other hand were noticed for extracted width greater than 700 m. Attempt of an explanation is made.
• The existing N-S tectonic compression reduces the magnitudes of subsidence and increases the horizontal displacements.
• Comparison between the numerical modelling and the analytical model of Baochen for subsidence prediction indicates that the curve forms match qualitatively.

REFERENCES

Arcamone, J. 1980. Méthodologie d'étude des affaissements miniers en exploitation totale et partielle. *Thèse de Doc. INPL.* 99p.
Bandis, S.C. Lumsden, A.C. & Barton, N.R. 1983. Fundamentals of rock joint deformation. *Int. J. Rock Mech. Min. Sci & Geomech. Abstr.* Vol. 20, N°6, pp. 249-268.
Baochen, L. 1993. Ground surface movements due to underground excavation in the People's Republic of China, *Compressive Rock Engng.* Hudson (ed.), Vol. 4, pp.781-817.
Gaviglio, P. 1985. A fault and stress field analysis in a coal mine (Gardanne, Bouches du Rhone, France). 113: 349-366, *Tectonophysics.*
Gaviglio, P. 1987. Conséquences de l'évolution structurale sur les caractéristiques physiques des calcaires fuvéliens du bassin de l'Arc (Bouches du Rhône, France): fracturation, propriétés mécaniques, états de contrainte. *Revue de Géologie Méditerranéenne,* XIV, 3: pp. 221-232.
Gaviglio, P. Revalor, R. Piguet, J.P. & Dejean, M. 1990. Tectonic structures, strata properties and rockburst occurrence in French coal mine. *Rockburst and Seismicity in Mines,* Fairhurst (ed.), 289-293. Rotterdam: Balkema.
Kulatilake, P.H.S.W. Ucpirti, H. Wang, S. Radberg, G. & Stephansson, O. 1992. Use of the distinct element method to perform stress analysis in rock with non-persistent joints and to study the effect of joint geometry parameters on strength and deformability of rock masses. *Rock Mech. and Rock Engng.* Vol. 25, N°4. pp. 253-284.
Mamane, I. 1995. Modélisation à grande échelle de l'influence de la fracturation sur les contraintes in situ et les affaissements miniers. *Thèse de Doc. INPL.* 202p.
Whittaker, N.B. & Reddish, D.J. 1993. Subsidence behavior of rocks structures, *Compressive Rock Engng.* Hudson (ed.), Vol. 4, pp.751-780.